

X-ray emission from isolated neutron stars: latest results from XMM-Newton, NICER and eROSITA

M. Rigoselli

*INAF OA-Brera, via Brera, 28
Milano 20121, Italy*

and

*INAF IASF-Milano, via A. Corti, 15
Milano 20133, Italy
michela.rigoselli@inaf.it*

The X-ray spectra of isolated neutron stars (INSs) typically include a thermal component, that comes from the cooling surface, and a non-thermal component, produced by highly-relativistic particles accelerated in the stellar magnetosphere. Hot spots from returning currents can also be detected.

Middle-aged pulsars exhibit a mixture of these components, but other flavours of INSs, that show a large variety of physical parameters (such as spin period, magnetic field and age) emit only thermal X-rays. Typically, these stars are detected either in large serendipitous datasets from pointed X-ray observations or from searches in the data of all-sky surveys.

The connection between these thermally-emitting INSs, the ordinary pulsars, and the new emergent class of pulsars characterized by a long period, that do not show X-ray emission despite their high magnetic field, is one of the current challenges in the study of neutron stars.

In this contribution I will review the latest results on several objects belonging to various INS classes, such as the XDINS RX J1856.5–3754, the enigmatic Calvera, the long period PSR J0250+5854 and the new thermal INS candidates, obtained with the X-ray observatories *XMM-Newton*, *NICER* and *eROSITA*.

1. The Isolated Neutron Stars zoology

Neutron stars were first discovered as radio pulsating sources in 1967¹, and in the following half a century more than 3700 have been recorded^{a2}. They have been discovered mainly by the detection of their pulsed non-thermal emission, at wavelengths ranging from radio to γ -rays, and may be isolated stars or members of a binary system.

The energy that sustains pulsar emission is supplied by their fast rotation, via the braking operated by their intense magnetic field. At the beginning of their life, pulsars spin with periods P_0 of the order of milliseconds, and they gradually slow down. Under the assumption of a constant, dipolar magnetic field and that the current period P is larger than P_0 , three characteristic quantities can be inferred from P and its derivative \dot{P} : the so-called spin-down luminosity

$$\dot{E}_{\text{rot}} = 4\pi^2 I_{\text{NS}} \dot{P} P^{-3}, \quad (1)$$

^a<https://www.atnf.csiro.au/research/pulsar/psrcat/>.

2

where $I_{\text{NS}} \approx 10^{45} \text{ g cm}^2$ is the moment of inertia of the neutron star, the dipolar magnetic field on the surface

$$B_{\text{dip}} \approx 3.2 \times 10^{19} (P\dot{P})^{1/2} \text{ G}, \quad (2)$$

and the characteristic age

$$\tau_c = \frac{P}{2\dot{P}}. \quad (3)$$

P and \dot{P} play a fundamental role in characterizing the pulsar properties, and the neutron star population is usually represented in the $P - \dot{P}$ diagram (shown in Figure 1), as the ordinary stars are represented in the Hertzsprung-Russell diagram; the different classes of neutron stars are placed on different zones of the diagram.

In the following, I will review the main X-ray properties of isolated neutron stars (INs) ³⁻⁶ that are powered by rotation (Section 1.1) or by secular cooling (Section 1.2), and recent discoveries that assess the links between the different classes (Sections 2 and 3).

1.1. *Rotation-powered pulsars*

Rotation-powered pulsars (RPPs) are the bulk of INs and are detected thanks to their pulsed emission. Nowadays more than 3500 RPPs are known, and they have been detected from the radio band to the very-high energy γ -rays (see e.g. the recent result on Vela pulsating emission up to 20 TeV ⁸). RPPs fill the central region of the $P - \dot{P}$ diagram (Figure 1, black dots); a newborn pulsar appears in the top-left corner and, according to the magnetic-dipole braking model, it evolves along the B_{dip} constant lines (dashed), crossing the τ_c constant lines (dotted). The bottom-right corner of the plot is empty because when a pulsar crosses the so-called “death line” ⁹, it is too old and too slow to sustain the required potential drop for pair production in the vacuum gap ^{10,11}.

Actually, a growing number of pulsars with $P > 12 \text{ s}$ that crosses the death line (see Figure 1, purple triangles) has been discovered in the last few years (see Section 2.1). It should be noted that there are many possible death lines (see the discussion in Suvorov & Melatos 2023 ¹²), which differ for the emission model (inner vacuum-gap curvature radiation or space-charge-limited flow), the nature of the seed γ -ray photons for pair production (curvature radiation or Inverse Compton), the magnetic field configuration (dipolar, multipolar, twisted) and the intensity of the frame dragging. Nevertheless, the observed timing and polarization properties, as well as the radio and X-ray manifestations, challenge the current picture of INs.

RPPs can be further divided into old, fast spinning pulsars (the millisecond pulsars ¹³), and young, strongly magnetized pulsars (the high-B pulsars ¹⁴). The millisecond pulsars are old pulsars that nonetheless have short and stable periods ($P \lesssim 10 \text{ ms}$, $\dot{P} \lesssim 10^{-18} \text{ s s}^{-1}$, see Figure 1, orange dots) that have been spun up through the accretion of matter from the binary companion over a prolonged phase

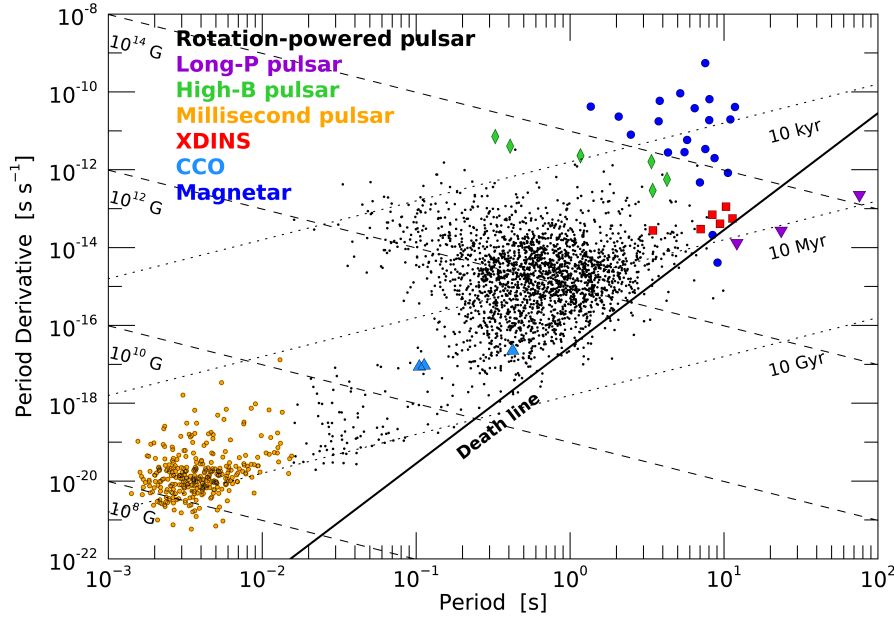


Fig. 1. $P - \dot{P}$ diagram of pulsars. The bulk of the pulsar population is made up of the rotation-powered pulsars (black dots), sub-divided into long-P pulsars (purple triangles), millisecond pulsars (orange dots), and high-B pulsars (green diamonds). The other classes of INs plotted here are the magnetars (blue dots), the XDINSs (red squares) and the CCOs (light blue triangles). Lines of equal characteristic age (dotted, $10^4 - 10^{10}$ yr) and equal dipole magnetic field (dashed, $10^8 - 10^{14}$ G) are indicated. The radio pulsar death line $B/P^2 = 1.7 \times 10^{11}$ G s $^{-2}$ of Bhattacharya et al. 1992⁷ is also shown. The data are taken from the ATNF Pulsar Catalogue, version 2.5.1².

lasting even giga-years in their evolutionary history. The majority of them still have a companion star and emit powerful non-thermal emission in radio, X- and γ -ray bands, and sometimes an additional thermal X-ray component from heated polar caps.

The high-B pulsars have magnetic fields higher than the quantum critical field

$$B_{\text{QED}} = \frac{m_e^2 c^3}{e \hbar} \approx 4.4 \times 10^{13} \text{ G} \quad (4)$$

(see Figure 1, green diamonds), and they do not constitute a separated class of INs, but they act as ordinary pulsars most of the time, and suddenly show bursting phenomena as the magnetars or share the spectral properties of the XDINSs (see Section 2.2).

1.2. Cooling neutron stars

Neutron stars also shine in the optical/UV/X-ray frequency range thanks to their hot surface. Thermal emission can be detected from the cooling surface and from

hot spots heated by returning currents (see Potekhin et al. 2020¹⁵ and references therein). Typically, this component is less pulsed and less beamed than the non-thermal one, which increases the likelihood of serendipitous discoveries. Recent discoveries of new thermally-emitting INS candidates are reported in Section 2.3.

Among thermally-emitting INSs, there are two small groups that do not show magnetospheric activity at any frequency^{16,17}, and it is not clear yet if they are a different flavor of INS or they are just seen with an unfavorable line of sight. They have been discovered thanks to their high X-ray-to-optical flux ratio (the X-ray-dim isolated neutron stars, XDINSs^{18,19}) or as hot sources at the center of supernova remnants (the central compact objects, CCOs^{20,21}). Their thermal X-ray spectra can also show absorption lines at a few hundreds of eV. If these lines are interpreted as cyclotron features, the estimated magnetic fields are

$$B_{\text{cyc,e}} = E_{\text{abs}} \frac{m_e c}{\hbar e} (1+z)^{-1} \approx \frac{E_{\text{abs}}}{100 \text{ eV}} 7.2 \times 10^9 \text{ G.} \quad (5)$$

in the case of electrons, or

$$B_{\text{cyc,p}} = E_{\text{abs}} \frac{m_p c}{\hbar e} (1+z)^{-1} \approx \frac{E_{\text{abs}}}{100 \text{ eV}} 1.3 \times 10^{13} \text{ G.} \quad (6)$$

in the case of protons.

The XDINSs are seven INSs discovered in the nineties by the *ROSAT* satellite and soon gained the nickname of “Magnificent Seven”. They have spin periods in the range 3 – 12 s and period derivatives of a few $10^{-14} \text{ s s}^{-1}$ (see Figure 1, red squares), which result in characteristic ages of $\tau_c \sim 1 - 4 \text{ Myr}$ and magnetic fields of the order of a few 10^{13} G . Their very soft ($kT \lesssim 100 \text{ eV}$) X-ray spectra are well reproduced by a simple blackbody with little interstellar absorption, with the additional presence of broad absorption lines at 200 – 400 eV in most sources^{22–25}, and narrow, phase-variable ones in few cases^{26,27}.

The CCOs form a class that counts a dozen objects. Their thermal spectra have high temperatures (200 – 500 eV) and very small emitting radii (ranging from 0.1 to a few km), and can show absorption features at 700 – 800 eV^{28,29}. Currently there are only three pulsating CCOs (see Figure 1, light blue triangles), that have periods of 0.1 – 0.4 s^{30–32} and spin derivatives of about $10^{-17} \text{ s s}^{-1}$ ^{20,33}, from which weak dipole magnetic fields ($B_{\text{dip}} \sim 10^{10} \text{ G}$) and high characteristic ages ($\tau_c \sim 10^8 \text{ yr}$) are derived. This is at variance with the supernova remnant (SNR) associations, and the reason could be that the approximation of Eq. 3 is no longer valid because these sources have $P \approx P_0$. One remarkable CCO in SNR RCW 103 shows a 6.7-hr X-ray periodicity of yet unknown origin as well as distinctly magnetar-like behavior^{34,35}. Such long spin periods in young non-accreting objects can be explained in a model where a strong magnetic field of the star interacts with a fallback disc (see also Section 2.1).

2. New discoveries in the X-ray band

2.1. Long period pulsars

There is a new emergent class of pulsars characterized by a long period: PSR J2251–3711 ($P \approx 12.1 \text{ s}^{36}$), PSR J1903+0433 ($P \approx 14.0 \text{ s}^{37}$), PSR J0250+5854 ($P \approx 23.5 \text{ s}^{38}$), and PSR J0901–4046 ($P \approx 75.9 \text{ s}^{39}$). They are located near magnetars and XDINSs on the $P - \dot{P}$ diagram, therefore they are characterized by high $B_{\text{dip}} \sim 10^{13-14} \text{ G}$ and long $\tau_c \sim 10^7 \text{ yr}$, but on the contrary they are radio sources without any X-ray counterpart.

The upper limits on the X-ray luminosity confirm that they are rather old neutron stars⁴⁰. Tan et al. 2023⁴¹ report the deep *XMM-Newton* observation of PSR J0250+5854. In almost 100 ks of *XMM-Newton*/EPIC exposure time, a 3σ upper limit on the count rate of $9 \times 10^{-4} \text{ cts s}^{-1}$ was derived. Assuming a pure thermal emission, an absorption $N_{\text{H}} = 1.36 \times 10^{21} \text{ cm}^{-2}$ and a distance of $1.6 \pm 0.7 \text{ kpc}$, the bolometric luminosity upper limit shown in Figure 2 was derived. This value is below the luminosities of most of the XDINSs, suggesting that PSR J0250+5854 is unlikely a member of this class unless it has a relatively low surface temperature ($kT < 50 \text{ eV}$). A similar conclusion applies if we compare PSR J0250+5854 with the low-B magnetars, such as SGR 0418+5729⁴², whose thermal luminosity comes from hot spots maintained by the bombardment of energetic particles carried by magnetospheric currents. In this case, the putative hot spot of PSR J0250+5854 should be colder than 200 eV.

An even more exotic class is composed by transient/intermittent radio sources that, when are active, show strongly polarized coherent radio pulses on timescales of thousands of seconds. The first and more famous object of this class is GLEAM-X J162759.5–523504.3, that showed pulsating radio emission with a period $P \approx 18$ minutes⁴³, then GPM J1839–10 ($P \approx 22$ minutes⁴⁴), ASKAP J1935+2148 ($P \approx 54$ minutes⁴⁵), GLEAM-X J0704–37 ($P \approx 2.9$ hours⁴⁶) and ASKAP J1839–0756 ($P \approx 6.45$ hours⁴⁷) followed. The period derivative of these objects has not been measured yet, but the upper limits set incredibly strong $B_{\text{dip}} < 10^{15-16} \text{ G}$. The variable flux and pulse profile, and the huge radio luminosity $\gtrsim \dot{E}_{\text{rot}}$, indicate that the emission is not generated purely by spin down but that an additional source of energy, possibly magnetic, is needed.

The properties of these ultra-long period radio sources resemble in some sense those of the 6.7 hr pulsating source at the center of SNR RCW 103^{34,35}, and those of the radio active magnetars⁴⁸. They have also been considered as candidate fast radio bursts progenitors⁴⁹, especially after the discovery of repeating fast radio bursts (see, e.g., the case of FRB 180916.J0158+65 having a periodicity of about 16.35 days⁵⁰).

The nature of ultra-long period radio sources is still debated. They could be magnetars that emit coherent radio emission despite extreme values of P and \dot{P} thanks to alternative sources of power, such as magnetospheric twists powered by plastic crustal motion⁵¹, or they could be magnetic white dwarfs with dipolar spin-

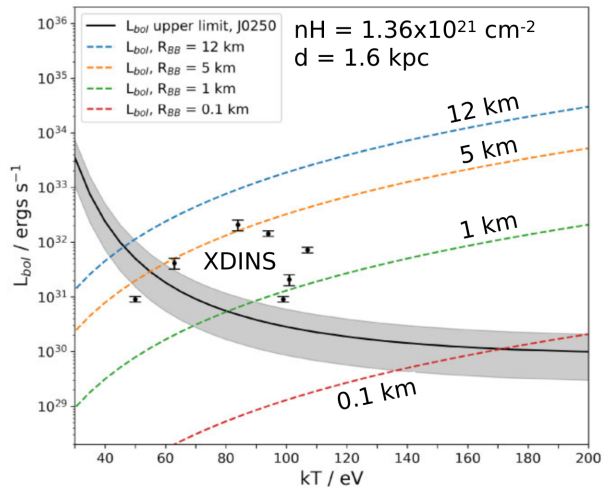


Fig. 2. Bolometric luminosity upper limit of PSR J0250+5854 for various values of blackbody temperature between 30 and 200 eV. The shaded region is the uncertainty in the computed upper limit, considering $d = 1.6 \pm 0.7$ kpc. The dashed colored lines are the expected bolometric luminosity of a blackbody of emitting radius 12, 5, 1, and 0.1 km, respectively. Adapted from Tan et al. 2023⁴¹.

down emission enhanced by the intra-binary shock with the wind of the companion star⁵², similarly to the models that explain the radio emission of AR Sco ($P \approx 1.95$ min in a 3.5 hr orbit⁵³) and J1912–4410 ($P \approx 5.3$ min in a 4 hr orbit⁵⁴). However, no optical/IR counterparts of the ultra-long period radio sources have been detected so far, ruling out the existence of a hot companion star⁵⁵. One remarkable exception is the recently-discovered GLEAM-X J0704–37: its high Galactic latitude and its M3-dwarf star companion, detected in the optical band, exclude the magnetar interpretation for this system⁴⁶.

2.2. Links between the classes of XDINS and RPP

The most recent discoveries in the X-ray manifestations of INSs have narrowed the differences between the classes of XDINS and RPP. These concern the radio high-B pulsar PSR J0726–2612, that has similar timing and spectral properties of XDINSs, and the detection of non-thermal emission of two XDINSs.

PSR J0726–2612 is slowly rotating ($P \approx 3.4$ s), highly magnetized ($B_{\text{dip}} = 3 \times 10^{13}$ G) radio pulsar: its timing parameters are in the range of those of the XDINSs, but it does show radio pulsations. The similarity with the XDINSs was reinforced by X-ray observations with the *Chandra*⁵⁶ and *XMM-Newton*⁵⁷ satellites, that revealed a purely soft thermal spectrum (temperatures $kT_1 = 74_{-11}^{+6}$ eV and $kT_2 = 140_{-20}^{+40}$ eV) plus an absorption Gaussian line with the line placed at $E = 390_{-30}^{+20}$ eV and with a broadening of $\sigma = 80_{-20}^{+30}$ eV. The inferred magnetic field is $B \approx 5 \times 10^{13}$ G

(see Eq. 6), in good agreement with the dipole magnetic field.

The X-ray pulse profile is sinusoidal and double-peaked, with a pulsed fraction of 30% (see Figure 3, left panel). It cannot be easily reproduced by simple models based on blackbody emission, and the best match with the data was obtained assuming emission from two antipodal hot spots with an effective temperature of 0.5 MK reprocessed by a magnetized atmosphere model. The inferred geometry ($\Omega - \mu \approx \Omega - \text{LOS}$) (where Ω and μ are the rotation and the magnetic axes, respectively, and the LOS is the direction of the line of sight) allows the detection of radio emission, while it is at variance with those of other XDINSs (RX J0720.4–3125⁵⁸ and RX J1308.6+2127⁵⁹). This discrepancy might explain why PSR J0726–2612 is detected in the radio band, while the two XDINSs are not.

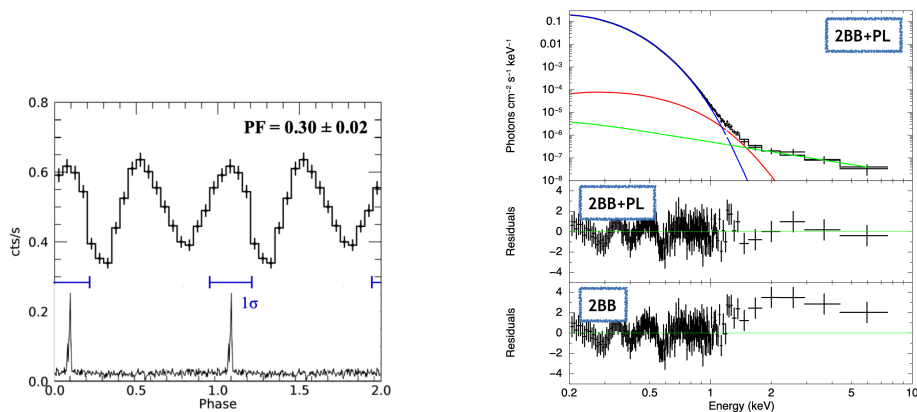


Fig. 3. Left panel: X-ray and radio pulse profile of PSR J0726–2612. Adapted from Rigoselli et al. 2019⁵⁷. Right panel: X-ray spectrum of RX J1856.5–3754 obtained with *XMM-Newton* data. The best-fitting model with two blackbody (blue and red) and a power-law (green) components is superimposed in the top panel. The two bottom panels show the residuals for the two-blackbody plus power law fit (2BB+PL) itself and for the two blackbody (2BB) fit, which yield unsatisfactory residuals at $E > 1$ keV. On the contrary, the residuals below 0.6 keV are at a level $< 2\%$, well below the instrument effective area uncertainties. Adapted from De Grandis et al. 2022⁶⁰.

The soft X-ray pulsar RX J1856.5–3754 is the brightest ($F_X \approx 1.5 \times 10^{-11}$ erg s⁻¹ cm⁻²⁶¹) and closest ($d = 123_{-15}^{+11}$ pc⁶²) member of the XDINS class. Its pulsation, with $P \approx 7.05$ s⁶³ and $\dot{P} \approx 3 \times 10^{-14}$ s s⁻¹⁶⁴, was detected despite a very small pulsed fraction $\text{PF} \approx 1.2\%$. The timing parameters yield $\dot{E}_{\text{rot}} = 3.4 \times 10^{30}$ erg s⁻¹, $\tau_c = 3.7 \times 10^6$ yr and $B_{\text{dip}} = 1.5 \times 10^{13}$ G.

The brightness, simple spectrum, and steadiness of its emission make RX J1856.5–3754 an ideal target for the calibration of *XMM-Newton*, that observed it about every six months since 2002. Using all the 2002–2022 data from the *XMM-Newton*/EPIC-pn camera, De Grandis et al. 2022⁶⁰ obtained a 0.3–7.5 keV spectrum having 1.43 Ms of net exposure time, that showed a hard excess with respect

to the pure blackbody emission^{65,66}. They report a best fit made up of the sum of two blackbodies (temperatures $kT_1 = 61.9 \pm 0.1$ eV and $kT_2 = 138 \pm 13$ eV, radii $R_1 = 4.92^{+0.04}_{-0.06}$ km and $R_2 = 31^{+8}_{-16}$ m) and a power law (photon index $\Gamma = 1.4^{+0.5}_{-0.4}$, flux in the 2 – 8 keV band of $(2.5^{+0.7}_{-0.6}) \times 10^{-15}$ erg s⁻¹ cm⁻² (see Figure 3, right panel).

The luminosity of the non-thermal component corresponds to 10^{-3} times the spin-down power \dot{E}_{rot} . This value is consistent with what is observed in rotation powered X-ray pulsars with higher \dot{E}_{rot} ⁶⁷. Hints for pulsations above 2 keV were also reported, so that a magnetospheric origin for this component appears as the most natural option.

De Grandis et al. 2022⁶⁰ analyzed also 20 years of *XMM-Newton* data of RX J0420.0–5022, the XDINS having the second highest \dot{E}_{rot} of the class. They found a hard excess that can be fit either with a second blackbody of a power law, or their sum. Also in this case, the putative non-thermal component would have an efficiency $L_{\text{PL}}/\dot{E}_{\text{rot}} \sim 10^{-3}$. If we assume the same efficiency, we expect that the other five XDINSs could show a similar non-thermal component with a flux $F_{\text{PL}} \lesssim 10^{-16}$ erg s⁻¹ cm⁻². This level of flux is beyond the sensitivity of the current facilities, but it maybe a target for future X-ray missions, such as *NewAthena*⁶⁸.

2.3. Increasing the sample of INSs

The storage of several hundreds of ks of *XMM-Newton* and *Chandra* pointings, as well as the increased sensitivity of the all sky survey in the soft X-ray band provided by *eROSITA*, allowed us to discover new INS candidates even in the absence of pulsations. This could be caused by an unfavorable orientation of the rotation and magnetic axes, or by the intrinsic lack, or faintness, of non-thermal magnetospheric emission.

Among the several hundreds of thousands of unassociated X-ray sources, thermally-emitting INSs are point like and have a constant long-term emission, characterized by a soft, thermal spectrum, with a high X-ray-to-optical flux ratio (F_X/F_O). The soft thermal spectrum can be constrained even without a spectral fit using a hardness-ratio plot in the soft X-ray band (Figure 4, left panel). This selection excludes the most abundant class of X-ray sources, i.e. the active galactic nuclei (AGN). The second class is composed by main sequence stars, bright in the X-rays but even brighter in the optical band. Therefore, a cut of $F_X/F_O > 10^3$ can select only the INSs (Figure 4, right panel).

The most promising INS candidates are 2XMM J104608.7–594306^{69,70} and 4XMM J022141.5–735632^{71,72}, plus about 30 sources announced in the recent data release of the first *eROSITA* catalog⁷³. The ultimate proof for a neutron star association is the detection of pulsation: eRASSU J131716.9–402647⁷⁴ and eRASSU J065715.3+260428⁷⁵ were targeted by *XMM-Newton* and *NICER*, and pulsations with $P \approx 12.76$ s and $\dot{P} < 8 \times 10^{-11}$ ss⁻¹ (J1317) and $P \approx 0.261$ s and $\dot{P} = 6^{+11}_{-4} \times 10^{-15}$ ss⁻¹ (J0657) were detected. Absorption features in the

thermal X-ray spectrum were measured at several hundreds of eV implying a magnetic field of $B \sim 10^{13-14}$ G. Deep optical observations with VLT put even more constraining magnitude limits of $m > 27.5$ (J1317) and $m > 27.3$ (J0657), implying $F_X/F_O > 10^4$.

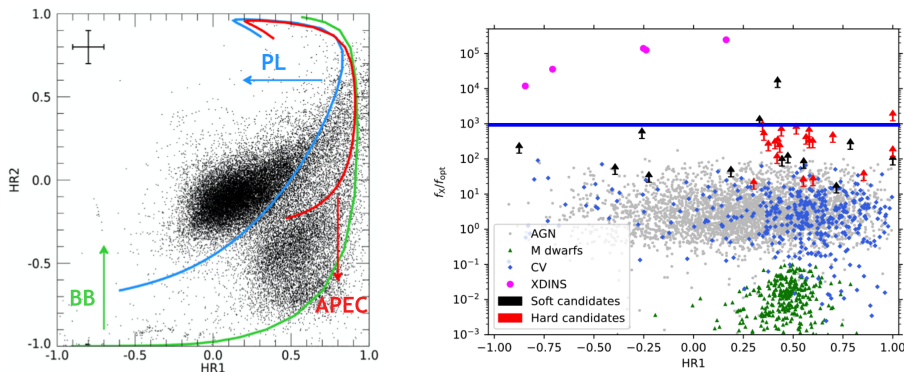


Fig. 4. Left: HR_1 – HR_2 plot of the the point-like 4XMM-DR9 sources. The considered energy ranges are 0.2 – 0.5, 0.5 – 1 and 1 – 2 keV. Colored lines represent the expected values for analytic models (blue line: PL, $\Gamma \lesssim 4$; red line: APEC, $kT \lesssim 1.05$ keV, 0.5 solar abundance; green line: BB, $kT = 0.05$ keV) convolved with the instrumental response function. All the lines are obtained varying N_H from 0 to 10^{23} cm^{-2} using the TBABS model. Credits to Rigoselli et al. 2022⁷¹. Right: F_X/F_O as a function of HR_1 for all the soft (black) and hard (red) candidates from the *eROSITA* first catalog. The known XDINSs are also shown with magenta dots. The most prevalent contaminants are M dwarfs (green), cataclysmic variable stars (blue) and AGNs (grey), that are all below a threshold value of 10^3 (blue line). Credits to Kurpas et al. 2024⁷³.

Among the thermal-emitting INSs, Calvera (1RXS J141256.0+792204) is one of the most enigmatic sources because its timing and spectral properties do not fit easily with those of the known classes of INSs. It was discovered in the *ROSAT* all sky survey as a soft X-ray source with high F_X/F_O , qualifying it as an INS candidate⁷⁶. Its spectral properties (emission of thermal X-rays only, absence of radio and γ -ray counterparts) resemble those of XDINSs and CCOs, and for these reasons it was initially considered as a possible new member of the “Magnificent Seven”; however, it was later discovered that Calvera has a spin period of 59 ms⁷⁷ and is spinning down at a rate $\dot{P} \approx 3.2 \times 10^{-15}$ s s^{-1} ⁷⁸. These timing parameters give a characteristic age $\tau_c = 2.9 \times 10^5$ yr and a dipole magnetic field $B_{\text{dip}} = 4.4 \times 10^{11}$ G, similarly to middle-aged RPPs. For this reason it was nicknamed “Calvera”.

A magnetized hydrogen atmosphere model, covering the entire star surface and having an anisotropic temperature map, provides a good description of the phase-resolved spectra and energy-dependent pulsed fraction observed by *NICER*⁷⁹. The inferred distance $d \approx 3.3$ kpc, coupled with a Galactic latitude $b \approx +37^\circ$, provides an unusually high height above the Galactic disk ($z \approx 2$ kpc, see Figure 5). This

supports the idea that Calvera was born in the Galactic halo, most likely from the explosion of a run-away massive star or, possibly, in a more unusual event involving a halo star, such as, e.g., the accretion induced collapse of a white dwarf.

Zane et al. 2011⁷⁷ reported the presence of diffuse X-ray emission about 13' west of Calvera, with spectral properties consistent with a SNR; recently, radio⁸⁰ and γ -ray^{81,82} counterparts of this remnant were discovered. The association between the pulsar and the SNR was recently confirmed with the measurement of a proper motion of $78.5 \pm 2.9 \text{ mas yr}^{-1}$ pointing away from the center of the ring⁸³. These findings imply that Calvera is much younger than inferred from its timing parameters, reinforcing the similarities with the CCO class.

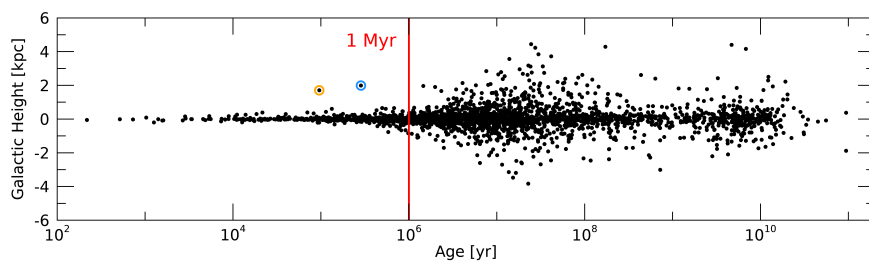


Fig. 5. Height on the Galactic plane as a function of characteristic age for all the Galactic INs (excluded those in globular clusters). The majority of stars younger than 1 Myr is less than ~ 500 pc distant from the plane; the only two exceptions are PSR J1951+4724 (orange, $b \approx 10^\circ$, $d \approx 9.4$ kpc or $d \approx 6.1$ kpc inferred from the radio dispersion measure and the models YMW16⁸⁴ and NE2001⁸⁵, respectively) and Calvera (blue, $b \approx 37^\circ$, $d \approx 3.3$ kpc inferred from fitting the thermal X-ray spectrum⁷⁹). The data are taken from the ATNF Pulsar Catalogue, version 2.5.1².

3. Multipolar and toroidal magnetic field

In this section I will report the growing evidence that the magnetic field has complicated field lines (multipolar and toroidal components) in the crust and above the surface also in ordinary RPPs: these concern the polar cap size (Section 3.1), the presence of absorption features in the soft X-ray band (Section 3.2), and the thermal surface map that can be inferred from timing and spectral analysis (Section 3.3).

3.1. Polar cap size

The study of neutron star heating by backward-accelerated particles is of particular interest for the study of particle acceleration in the pulsar magnetosphere^{86–89}. In the classical dipolar scenario, the hot spots are identical and antipodal, are situated in correspondence of the magnetic poles and have a size $R_{\text{dip}} = \sqrt{2\pi R_*^3 / Pc} \approx 145 P_{1s}^{-1/2}$ m. Several *XMM-Newton* and *Chandra* observations have been devoted

to measure the characteristics of the hot spots of the brightest old pulsars, that have cooled down enough so that this contribution can be disentangled from the emission of the cooling surface, no longer relevant in the X-ray band. The emitting radii of the hot spots, inferred with blackbody fits, are a few meters only, and not all the pulse profiles are symmetric^{90–94}.

It was proposed^{90,95} that such a small emitting area can be explained if we consider that, close to the star surface, the magnetic field is stronger than the dipolar field and described by multipolar components:

$$B_{\text{PC}} = B_{\text{dip}} \left(\frac{R_{\text{dip}}}{R_{\text{PC}}} \right)^2 \approx 10^2 B_{\text{dip}} \quad (7)$$

and the conservation of the magnetic flux through the polar cap area explain why we observe $R_{\text{PC}} \sim 10 - 40$ m. The asymmetry of the pulse profile also denotes that the geometry of the magnetic field close to the surface may be off-centered, and this would imply two caps that are non-identical, non-antipodal, and out of phase with respect to the radio main peak. Recent results obtained with *NICER*^{96–99} also report evidence for non-dipolar magnetic fields, but they refer to the older millisecond pulsars that have $B_{\text{dip}} \sim 10^9$ G.

These discrepancies can also be addressed using more realistic thermal models, accounting for the effects of magnetic field on either a condensed surface or an atmosphere. It is well known that atmospheric models are spectrally harder than blackbodies, thus yielding best-fit temperatures a factor two lower and, as a consequence, larger emitting areas. For three pulsars, the latter are consistent with the dipole polar caps (PSR B0950+08¹⁰⁰, PSR B0823+26¹⁰¹, PSR B0943+10¹⁰²). However, these models depend on many more parameters than a simple blackbody, such as the chemical composition, the star mass and radius, the magnetic field, the system geometry, that in most cases are unknown and difficult to constrain due to relatively faint emission.

3.2. Absorption lines

As said in Section 1.2, cyclotron features are detected in the (thermal) X-ray spectra of particular classes of INSs, that have the appropriate magnetic field to produce electron or proton absorption lines, respectively. On the contrary, for the ordinary pulsars (with $B_{\text{dip}} \sim 10^{12}$ G) neither of the two conditions is met at the star surface and hence no analogous cyclotron features are expected in soft X-rays (Eqq. 5 and 6).

Nevertheless, in the last few years some ordinary RPPs (PSR J1740+1000¹⁰³, PSR B1133+16¹⁰⁴, and PSR B0656+14¹⁰⁵) showed evidence for the presence of features in their X-ray spectra at about ~ 500 eV. The case of PSR J1740+1000 is extremely intriguing because, after a glitch occurred in 2012, the X-ray spectrum has changed and the absorption lines seem to have disappeared¹⁰⁶.

If the electrons are responsible for such features, they must be located high in the magnetosphere, at several stellar radii above the stellar surface where the

dipole field is weaker ($B \propto (r/R_*)^{-3}$). Thus, the absorbed X-ray photons can be produced either on the surface or in the close magnetosphere. Alternatively, if the lines are attributed to protons close to the star surface, then a magnetic field $B = 4.5 \times 10^{13} \text{ G} \approx 10 \times B_{\text{dip}}$ is needed.

3.3. Surface temperature maps

In a strong magnetic field, electrons move more easily along the field lines than across them, making heat conductivity anisotropic. As a consequence, the magnetic field geometry determines the direction of heat conduction in INSs. In the radial magnetic field region of the envelope, heat is transported efficiently along the radial direction, establishing a thermal connection between the surface and the inner crust and core. Conversely, the regions with a nearly tangential magnetic field exhibit insulation and thermal disconnection from the hot core.

There are two quantities that are directly correlated to the temperature map and that can be inferred from X-ray observations: the pulsed fraction (PF) of the thermal component, and the deviation from a one-temperature thermal spectrum.

Several works^{107–109} showed that poloidal-dominated configurations can only yield symmetric pulse profiles and very low PFs unless the local emission is highly beamed. On the other hand, the anisotropies in the surface temperature profile induced by the presence of a strong, large-scale toroidal field generally produce single-peaked pulsed profiles, with a PF that can reach about the 50% even for purely isotropic local emission^{109–112}.

The majority of INS thermal spectra can be fitted with, at least, two blackbodies, that mimic the two extremes of a more complex temperature distribution. Rigoselli et al. 2022¹⁰⁶ showed that, with a few notable exceptions, the ratios of emitting radii ($R_{\text{hot}}/R_{\text{cold}}$) and temperatures ($T_{\text{hot}}/T_{\text{cold}}$) are very similar for all the families of INSs and are in the range $R_{\text{hot}}/R_{\text{cold}} \approx 0.03 - 0.3$ and $T_{\text{hot}}/T_{\text{cold}} \approx 2$. Thus it is difficult to interpret the hotter and colder components in terms of emission from hot spots and from the whole surface ($R \lesssim 200 \text{ m}$ and $R \sim 12 - 16 \text{ km}$, respectively), nor in terms of purely dipolar magnetic field, where a temperature contrast is expected to be below 1.5 (see also Yakovlev 2021¹¹³).

Acknowledgments

MR acknowledges INAF support through the Large Grant “Magnetars” (P.I. S. Mereghetti) of the “Bando per il Finanziamento della Ricerca Fondamentale 2022”.

References

1. Hewish, A., Bell, S. J., Pilkington, J. D. H., Scott, P. F., & Collins, R. A., *Nature* **217** (1968) 709.
2. Manchester, R. N., Hobbs, G. B., Teoh, A., & Hobbs, M., *AJ* **129** (2005) 1993.
3. Harding, A. K., *Frontiers of Physics* **8** (2013) 679.

4. Igoshev, A. P., Popov, S. B., & Turolla, R., *AN* **335** (2014) 262.
5. Kaspi, V. M., in *Pulsar Astrophysics the Next Fifty Years*, Weltevrede, P., Perera, B. B. P., Preston, L. L., & Sanidas, S., eds., vol. 337, (2018), pp. 3–8, DOI:10.1017/S1743921317010390.
6. Popov, S. B., *Universe* **9** (2023) 273.
7. Bhattacharya, D., Wijers, R. A. M. J., Hartman, J. W., & Verbunt, F., *A&A* **254** (1992) 198.
8. H. E. S. S. Collaboration, Aharonian, F., Ait Benkhali, F., et al., *Nature Astronomy* (2023) .
9. Chen, K. & Ruderman, M., *ApJ* **402** (1993) 264.
10. Baring, M. G. & Harding, A. K., *ApJ* **507** (1998) L55.
11. Baring, M. G. & Harding, A. K., *ApJ* **547** (2001) 929.
12. Suvorov, A. G. & Melatos, A., *MNRAS* **520** (2023) 1590.
13. Manchester, R. N., *JApA* **38** (2017) 42.
14. Ng, C. Y. & Kaspi, V. M., in *American Institute of Physics Conference Series*, Göğüş, E., Belloni, T., & Ertan, Ü., eds., vol. 1379, (2011), pp. 60–69, DOI:10.1063/1.3629486.
15. Potekhin, A. Y., Zyuzin, D. A., Yakovlev, D. G., Beznogov, M. V., & Shibano, Y. A., *MNRAS* **496** (2020) 5052.
16. Kondratiev, V. I., McLaughlin, M. A., Lorimer, D. R., et al., *ApJ* **702** (2009) 692.
17. Mignani, R. P., De Luca, A., Zharikov, S., et al., *MNRAS* **486** (2019) 5716.
18. van Kerkwijk, M. H. & Kaplan, D. L., *Ap&SS* **308** (2007) 191.
19. Turolla, R., in *Astrophysics and Space Science Library*, Becker, W., ed., vol. 357 of *Astrophysics and Space Science Library*, (2009), p. 141, DOI:10.1007/978-3-540-76965-1.7.
20. Gotthelf, E. V., Halpern, J. P., & Alford, J., *ApJ* **765** (2013) 58.
21. De Luca, A., in *Journal of Physics Conference Series*, vol. 932 of *Journal of Physics Conference Series*, (2017), p. 012006, DOI:10.1088/1742-6596/932/1/012006.
22. Haberl, F., Schwöpe, A. D., Hambaryan, V., Hasinger, G., & Motch, C., *A&A* **403** (2003) L19.
23. van Kerkwijk, M. H., Kaplan, D. L., Durant, M., Kulkarni, S. R., & Paerels, F., *ApJ* **608** (2004) 432.
24. Haberl, F., Motch, C., Zavlin, V. E., et al., *A&A* **424** (2004) 635.
25. Zane, S., Cropper, M., Turolla, R., et al., *ApJ* **627** (2005) 397.
26. Borghese, A., Rea, N., Coti Zelati, F., Tiengo, A., & Turolla, R., *ApJ* **807** (2015) L20.
27. Borghese, A., Rea, N., Coti Zelati, F., et al., *MNRAS* **468** (2017) 2975.
28. Bignami, G. F., Caraveo, P. A., De Luca, A., & Mereghetti, S., *Nature* **423** (2003) 725.
29. Gotthelf, E. V., Perna, R., & Halpern, J. P., *ApJ* **724** (2010) 1316.
30. Zavlin, V. E., Pavlov, G. G., Sanwal, D., & Trümper, J., *ApJ* **540** (2000) L25.
31. Gotthelf, E. V., Halpern, J. P., & Seward, F. D., *ApJ* **627** (2005) 390.
32. Gotthelf, E. V. & Halpern, J. P., *ApJ* **695** (2009) L35.
33. Halpern, J. P. & Gotthelf, E. V., *ApJ* **709** (2010) 436.
34. Rea, N., Borghese, A., Esposito, P., et al., *ApJ* **828** (2016) L13.
35. D’Ài, A., Evans, P. A., Burrows, D. N., et al., *MNRAS* **463** (2016) 2394.
36. Morello, V., Keane, E. F., Enoto, T., et al., *MNRAS* **493** (2020) 1165.
37. Han, J. L., Wang, C., Wang, P. F., et al., *RAA* **21** (2021) 107.
38. Tan, C. M., Bassa, C. G., Cooper, S., et al., *ApJ* **866** (2018) 54.

39. Caleb, M., Heywood, I., Rajwade, K., et al., *Nature Astronomy* **6** (2022) 828.
40. Rea, N., Coti Zelati, F., Dehman, C., et al., *ApJ* **940** (2022) 72.
41. Tan, C. M., Rigoselli, M., Esposito, P., & Stappers, B. W., *MNRAS* **520** (2023) 5960.
42. Rea, N., Israel, G. L., Pons, J. A., et al., *ApJ* **770** (2013) 65.
43. Hurley-Walker, N., Zhang, X., Bahramian, A., et al., *Nature* **601** (2022) 526.
44. Hurley-Walker, N., Rea, N., McSweeney, S. J., et al., *Nature* **619** (2023) 487.
45. Caleb, M., Lenc, E., Kaplan, D. L., et al., *Nature Astronomy* **8** (2024) 1159.
46. Hurley-Walker, N., McSweeney, S. J., Bahramian, A., et al., *ApJ* **976** (2024) L21.
47. Lee, Y. W. J., Caleb, M., Murphy, T., et al., *arXiv e-prints* (2025) arXiv:2501.09133.
48. Ronchi, M., Rea, N., Graber, V., & Hurley-Walker, N., *ApJ* **934** (2022) 184.
49. Beniamini, P., Wadiasingh, Z., & Metzger, B. D., *MNRAS* **496** (2020) 3390.
50. Chime/Frb Collaboration, Amiri, M., Andersen, B. C., et al., *Nature* **582** (2020) 351.
51. Cooper, A. J. & Wadiasingh, Z., *MNRAS* **533** (2024) 2133.
52. Rea, N., Hurley-Walker, N., Pardo-Araujo, C., et al., *ApJ* **961** (2024) 214.
53. Marsh, T. R., Gänsicke, B. T., Hümmelich, S., et al., *Nature* **537** (2016) 374.
54. Pelisoli, I., Marsh, T. R., Buckley, D. A. H., et al., *Nature Astronomy* **7** (2023) 931.
55. Beniamini, P., Wadiasingh, Z., Hare, J., et al., *MNRAS* **520** (2023) 1872.
56. Speagle, J. S., Kaplan, D. L., & van Kerkwijk, M. H., *ApJ* **743** (2011) 183.
57. Rigoselli, M., Mereghetti, S., Suleimanov, V., et al., *A&A* **627** (2019) A69.
58. Hambaryan, V., Suleimanov, V., Schwöpe, A. D., et al., *A&A* **534** (2011) A74.
59. Hambaryan, V., Suleimanov, V., Haberl, F., et al., *A&A* **601** (2017) A108.
60. De Grandis, D., Rigoselli, M., Mereghetti, S., et al., *MNRAS* **516** (2022) 4932.
61. Walter, F. M., Wolk, S. J., & Neuhäuser, R., *Nature* **379** (1996) 233.
62. Walter, F. M., Eisenbeiß, T., Lattimer, J. M., et al., *ApJ* **724** (2010) 669.
63. Tiengo, A. & Mereghetti, S., *ApJ* **657** (2007) L101.
64. van Kerkwijk, M. H. & Kaplan, D. L., *ApJ* **673** (2008) L163.
65. Yoneyama, T., Hayashida, K., Nakajima, H., Inoue, S., & Tsunemi, H., *PASJ* **69** (2017) 50.
66. Dessert, C., Foster, J. W., & Safdi, B. R., *ApJ* **904** (2020) 42.
67. Possenti, A., Cerutti, R., Colpi, M., & Mereghetti, S., *A&A* **387** (2002) 993.
68. Cruise, M., Guainazzi, M., Aird, J., et al., *arXiv e-prints* (2025) arXiv:2501.03100.
69. Pires, A. M., Motch, C., Turolla, R., Treves, A., & Popov, S. B., *A&A* **498** (2009) 233.
70. Pires, A. M., Motch, C., Turolla, R., et al., *A&A* **583** (2015) A117.
71. Rigoselli, M., Mereghetti, S., & Tresoldi, C., *MNRAS* **509** (2022) 1217.
72. Pires, A. M., Motch, C., Kurpas, J., et al., *A&A* **666** (2022) A148.
73. Kurpas, J., Schwöpe, A. D., Pires, A. M., & Haberl, F., *A&A* **687** (2024) A251.
74. Kurpas, J., Schwöpe, A. D., Pires, A. M., & Haberl, F., *A&A* **683** (2024) A164.
75. Kurpas, J., Pires, A. M., Schwöpe, A. D., et al., *arXiv e-prints* (2025) arXiv:2501.07347.
76. Rutledge, R. E., Fox, D. B., & Shevchuk, A. H., *ApJ* **672** (2008) 1137.
77. Zane, S., Haberl, F., Israel, G. L., et al., *MNRAS* **410** (2011) 2428.
78. Halpern, J. P., Bogdanov, S., & Gotthelf, E. V., *ApJ* **778** (2013) 120.
79. Mereghetti, S., Rigoselli, M., Taverna, R., et al., *ApJ* **922** (2021) 253.
80. Arias, M., Botteon, A., Bassa, C. G., et al., *A&A* **667** (2022) A71.
81. Xin, Y. & Guo, X., *ApJ* **941** (2022) 194.
82. Araya, M., *MNRAS* **518** (2023) 4132.

83. Rigoselli, M., Mereghetti, S., Halpern, J. P., Gotthelf, E. V., & Bassa, C. G., *ApJ* **976** (2024) 228.
84. Yao, J. M., Manchester, R. N., & Wang, N., *ApJ* **835** (2017) 29.
85. Cordes, J. M. & Lazio, T. J. W., *ArXiv Astrophysics e-prints* (2002) .
86. Harding, A. K. & Muslimov, A. G., *ApJ* **556** (2001) 987.
87. Harding, A. K. & Muslimov, A. G., *ApJ* **568** (2002) 862.
88. Cheng, K. S., Ho, C., & Ruderman, M., *ApJ* **300** (1986) 500.
89. Cheng, K. S., Ho, C., & Ruderman, M., *ApJ* **300** (1986) 522.
90. Gil, J., Haberl, F., Melikidze, G., et al., *ApJ* **686** (2008) 497.
91. Misanovic, Z., Pavlov, G. G., & Garmire, G. P., *ApJ* **685** (2008) 1129.
92. Hermsen, W., Hessels, J. W. T., Kuiper, L., et al., *Science* **339** (2013) 436.
93. Hermsen, W., Kuiper, L., Hessels, J. W. T., et al., *MNRAS* **466** (2017) 1688.
94. Igoshev, A. P., Tsygankov, S. S., Rigoselli, M., et al., *ApJ* **865** (2018) 116.
95. Gil, J., Melikidze, G. I., & Geppert, U., *A&A* **407** (2003) 315.
96. Bogdanov, S., Lamb, F. K., Mahmoodifar, S., et al., *ApJ* **887** (2019) L26.
97. Bilous, A. V., Watts, A. L., Harding, A. K., et al., *ApJ* **887** (2019) L23.
98. Riley, T. E., Watts, A. L., Bogdanov, S., et al., *ApJ* **887** (2019) L21.
99. Pétri, J., Guillot, S., Guillemot, L., et al., *A&A* **680** (2023) A93.
100. Zavlin, V. E. & Pavlov, G. G., *ApJ* **616** (2004) 452.
101. Hermsen, W., Kuiper, L., Basu, R., et al., *MNRAS* **480** (2018) 3655.
102. Rigoselli, M., Mereghetti, S., Turolla, R., et al., *ApJ* **872** (2019) 15.
103. Kargaltsev, O., Durant, M., Misanovic, Z., & Pavlov, G. G., *Science* **337** (2012) 946.
104. Rigoselli, M. & Mereghetti, S., *A&A* **615** (2018) A73.
105. Arumugasamy, P., Kargaltsev, O., Posselt, B., Pavlov, G. G., & Hare, J., *ApJ* **869** (2018) 97.
106. Rigoselli, M., Mereghetti, S., Anzuinelli, S., et al., *MNRAS* **513** (2022) 3113.
107. Greenstein, G. & Hartke, G. J., *ApJ* **271** (1983) 283.
108. Turolla, R. & Nobili, L., *ApJ* **768** (2013) 147.
109. Perna, R., Viganò, D., Pons, J. A., & Rea, N., *MNRAS* **434** (2013) 2362.
110. Pérez-Azorín, J. F., Miralles, J. A., & Pons, J. A., *A&A* **451** (2006) 1009.
111. Pérez-Azorín, J. F., Pons, J. A., Miralles, J. A., & Miniutti, G., *A&A* **459** (2006) 175.
112. Geppert, U., Küker, M., & Page, D., *A&A* **457** (2006) 937.
113. Yakovlev, D. G., *MNRAS* **506** (2021) 4593.